Imaging of Coulomb-Driven Quantum Hall Edge States

Keji Lai,[1,*] Worasom Kundhikanjana,[1] Michael A. Kelly,[1] Zhi-Xun Shen,[1] Javad Shabani,[2] and Mansour Shayegan[2]

[1]*Geballe Laboratory for Advanced Materials, Departments of Physics and Applied Physics, Stanford University,
Stanford California 94305, USA*
[2]*Departments of Electrical Engineering, Princeton University, Princeton New Jersey 08544, USA*

The edges of a two-dimensional electron gas (2DEG) in the quantum Hall effect (QHE) regime are divided into alternating metallic and insulating strips, with their widths determined by the energy gaps of the QHE states and the electrostatic Coulomb interaction. Local probing of these submicrometer features, however, is challenging due to the buried 2DEG structures. Using a newly developed microwave impedance microscope, we demonstrate the real-space conductivity mapping of the edge and bulk states. The sizes, positions, and field dependence of the edge strips around the sample perimeter agree quantitatively with the self-consistent electrostatic picture. The evolution of microwave images as a function of magnetic fields provides rich microscopic information around the $\nu = 2$ QHE state.

The quantum Hall effect (QHE) is among the few textbook examples where the experimental results are insensitive to imperfections in real materials and solely determined by fundamental physics constants. After decades of research, the exact quantization of the Hall resistance in a two-dimensional electron gas (2DEG) system under strong magnetic (B) fields is now understood by the localization of electronic states when the bulk of the 2DEG is close to integer or fractional Landau level (LL) filling factors (ν) [1]. Near the sample edges, however, the LLs bend up in energy due to the confining potential and intersect with the Fermi energy, resulting in alternating compressible (metal-like) and incompressible (insulator-like) strips [2–4]. In macroscopic samples, carriers propagating along the metallic edge channels are free from backscattering when scattered by impurities or inelastic events and, therefore, responsible for the topological robustness of the QHE [5]. The crucial role of edge states in the quantum Hall regime was recognized immediately after the proposal [2–5] and has continued to attract research interest in recent years [6,7].

Spatially resolved studies of the edge channels are usually challenging because most high mobility 2DEGs are located tens or even hundreds of nanometers below the surface of semiconductor heterostructures. Nevertheless, a number of novel designs, such as scanning gate microscopy [8–10], scanning single-electron transistor [11–13], and scanning charge accumulation microscopy [14–16], have shown compelling evidence of such edge modes by providing information on charge motion, surface potential, or local compressibility. Thorough studies of the local conductivity and the sizes of these edge channels, however, have not been achieved. In this Letter, we demonstrate the conductivity mapping of the bulk and edge states in a GaAs/AlGaAs 2DEG using a cryogenic microwave impedance microscope (MIM) [17–19]. Narrow strips with

either metallic or insulating screening properties are observed along edges of the sample as the system enters the QHE state. The evolution of the local conductivity distribution through the bulk filling factor $\nu_b = 2$ agrees with the self-consistent electrostatic calculation [3]. The imaging was performed without dc electrodes, vividly manifesting that the QHE edges are equilibrium states and do not depend on externally supplied currents.

The schematic setup of the variable-temperature (T) microwave microscope is shown in Fig. 1(a). An excitation power of 0.1–1 μW at 1 GHz is delivered to the shielded cantilever probe [20]. The reflected microwave is amplified by a cryogenic high electron mobility transistor (HEMT)
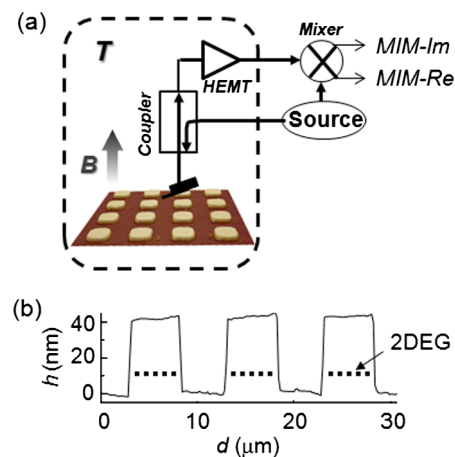

FIG. 1 (color online). (a) Schematic setup of the microwave microscope and the 3D rendered image of the sample surface. The reflected 1 GHz microwave from the cantilever tip is amplified and demodulated to form imaginary (MIM-Im) and real (MIM-Re) parts of the impedance maps. (b) A line profile of the surface topography through three dots. The 2DEG located 30 nm below the surface is indicated in the plot.

amplifier and demodulated by a room-temperature quadrature mixer. The two output signals are directly proportional to the imaginary (MIM-Im) and real (MIM-Re) parts of the tip-sample admittance (inverse impedance) during the scan. The electronics in this experiment were set such that a 1 aF admittance change corresponds to 14 mV in the output. The spatial resolution ~100 nm is limited by the tip diameter rather than the wavelength of the microwave [17]. In order to create physical boundaries, the 2DEG sample was patterned into isolated dots, each with a diameter of 6–7 μm. As shown in the atomic-force microscope line profile in Fig. 1(b), the 2DEG in the GaAs/AlGaAs interface (30 nm below the surface) was etched away between the dots. The bulk electron density ($n_b = 3 \times 10^{11}$ cm^{-2}) and mobility ($\mu = 5 \times 10^5$ cm^2/V s) at $T = 2$ K were measured by dc transport on an unpatterned piece from the same wafer. We note that only the local diagonal conductivity σ_{xx} is responsible for screening the in-plane radial microwave electric fields from the tip. The tangential current proportional to the Hall conductivity σ_{xy} is irrelevant since it does not contribute to the screening.

The origin of quantum Hall edge states is strictly quantum mechanical in nature. A semiclassical toy model, which intuitively suggests a conducting edge due to the cycloidal "skipping-orbit" motion, completely misses the essential physics of the QHE. The noninteracting one-electron picture is also inadequate here because it leads

to abrupt changes in density, prohibited by strong Coulomb penalty, where the Fermi level crosses a LL. When the electrostatic interaction is included [3], the density in real devices is depleted to zero near the sample edge by the confining potential, and rises smoothly toward n_b with a length scale determined by the depletion width (L). The Landau quantization $\varepsilon_N = (N + 1/2)\hbar\omega_C$, where N is the LL index and $\hbar\omega_C$ the cyclotron energy, gives rise to narrow constant-density regions with integer ν's. These highly resistive strips subdivide the edge into regions of different LL occupancy, commonly referred to as "edge states." The above scenario, including both the density profile and the energy diagram, is depicted in Figs. 2(a) and 2(b) using the actual sample parameters at $\nu_b = 2.31$. The depletion width $L = \varepsilon V_G/\pi n_b e \sim 110$ nm sets the density profile at the edge [3], where ε is the dielectric constant of GaAs, V_G the band gap, and e the electron charge. The $N = 0$ incompressible strip, which scales with $(a_B L)^{1/2}$ and $a_B \sim 10$ nm being the effective Bohr radius in GaAs, is narrower than the compressible edge, whose width scales with L. Because of the small spin splitting in GaAs, each LL is twofold degenerate at this temperature so the $\nu = 1$ incompressible strip is ignored.

Figures 2(c) and 2(d) show the MIM images at $\nu_b = 2.31$ ($B = 5.4$ T) and $T = 2.3$ K, with a typical line cut plotted in Fig. 2(e). In the extreme near-field regime, the tip-sample interaction is quasistatic and the impedance
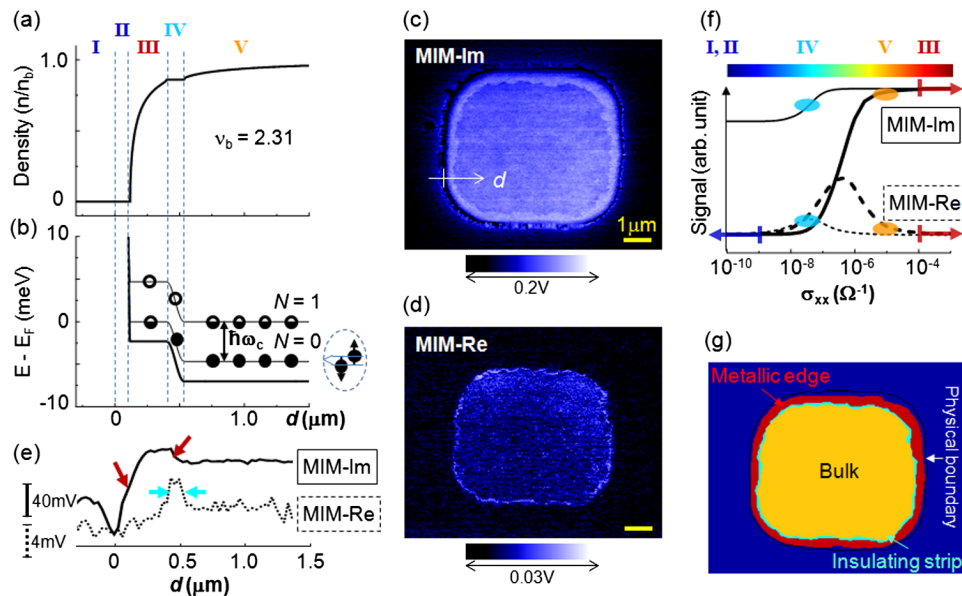

FIG. 2 (color online). (a) Density profile and (b) energy diagram near the sample edge at the bulk filling factor $\nu_b = 2.31$. The etched area (I), depletion region (II), metallic (III) and insulating (IV) strips, and the bulk (V) are labeled in the plot. The circles in the energy diagram (filled, half filled, and empty) show the level occupancy. (c) MIM-Im and (d) MIM-Re images at $B = 5.4$ T and $T = 2.3$ K. The full color scale corresponds to 0.2 V in MIM-Im and 0.03 V in MIM-Re. The scale bars are 1 μm. (e) Line cuts of the microwave data, labeled in (c). The vertical scales are 40 mV for the MIM-Im (solid line) and 4 mV for the MIM-Re data (dashed line). Rising and falling edges are indicated by arrows. (f) Results of the finite-element modeling, including the 2D axisymmetric analysis (thick solid and dashed lines) for the metallic edge and the bulk and the full 3D simulation (thin solid and dashed lines) for the insulating strip. (g) Idealized conductivity map combining the MIM images and the simulation.

changes as a function of local σ_{xx} can be computed by the finite-element analysis [18–20], as shown in Fig. 2(f). As detailed in the Supplemental Material [21], the MIM response is a weighted average of the complex dielectric constant in a volume probed by the rf electric fields, which localize well underneath the tip for conducting 2DEG and extend up to several hundred nanometers for insulating 2DEG. We can therefore use simple 2D axisymmetric simulation to interpret the data for the wide etched region, the metallic edge, and the bulk. For an insulating strip as narrow as ∼100 nm sandwiched between conducting regions, the full 3D modeling is required. Using Fig. 2(f) as a guide, the nonmonotonic conductivity distribution near the 2DEG edge is readily captured. First, the halo and the dark border near the physical boundary of the dot in Fig. 2(c) are topographic artifacts as the tip approaches and climbs up the 40 nm step edge (see the Supplemental Material [21]). The effect is less problematic when the tip moves toward the interior for a distance close to the tip size, which coincides with the nominal depletion width. The MIM-Im signal then rises to a high value and stays for ∼300 nm before dropping slightly into the bulk [22]. The high MIM-Im and low MIM-Re signals here indicate a high local $\sigma_{xx} > 1 \times 10^{-4} \ \Omega^{-1}$ of this band. The bulk conductivity

∼$1 \times 10^{-5} \ \Omega^{-1}$ is also determined by the lower MIM-Im and slightly higher MIM-Re signals than the metallic edge. Interestingly, in between these two regions, a narrow bright strip appears in the MIM-Re image, which can only be explained by the presence of a highly resistive channel with σ_{xx} in the order of 10^{-7}–$10^{-8} \ \Omega^{-1}$ [14]. This feature, which is also confirmed by 3D simulation with the tip scanning across a strip with fixed σ_{xx}, is not well resolved at higher T or near $\nu_b = 4$ (see the Supplemental Material [21]), presumably due to the lower resistivity of the strip under those conditions. Using standard edge detection schemes, boundaries of different regions are determined by the midpoints of the rising and falling edges, e.g., arrows in Fig. 2(e). We then construct an idealized conductivity map in Fig. 2(g), which vividly demonstrates the nontrivial physics of the QHE edge states.

The microwave images [23] around $\nu_b = 2$ are shown in Figs. 3(b)–3(l), with the corresponding B fields labeled on the transport data [Fig. 3(a)]. The conducting edge in MIM-Im and the resistive strip in MIM-Re are visible at $\nu_b = 2.60$ [Fig. 3(b)] and grow in width toward $\nu_b = 2$ [Figs. 3(c) and 3(d)]. Discernible MIM-Re "patch" signals are seen at $\nu_b = 2.12$ [Fig. 3(e)] in the bulk, indicative of the decrease of bulk conductivity here. Near the integer
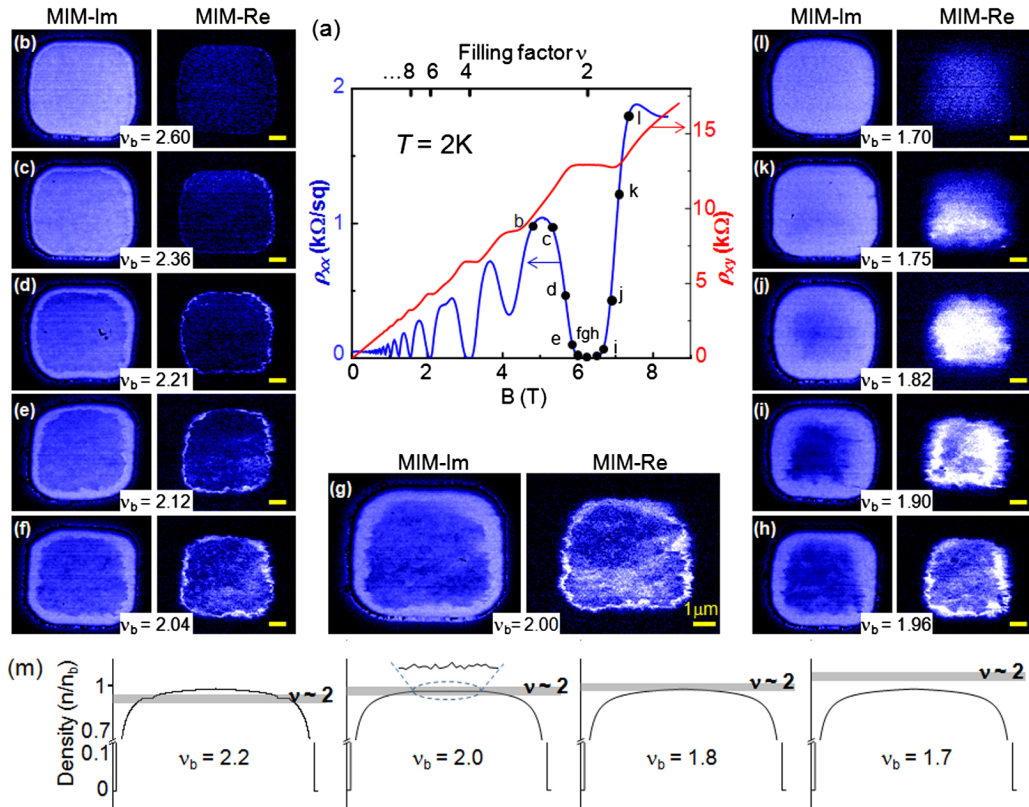

FIG. 3 (color online). (a) Longitudinal and Hall resistivity as a function of B or ν at 2 K. The corresponding B fields in (b)–(l) are labeled in the ρ_{xx} trace. (b)–(l) Counterclockwise from top left to top right, MIM images at $T = 2.3$ K as the B field increases from 4.8 T ($\nu_b = 2.6$) to 7.3 T ($\nu_b = 1.7$). All scale bars are 1 μm. The full color scales (not shown) are the same as Figs. 2(c) and 2(d). (m) From left to right, schematic density profiles across the center of the dots at $\nu_b = 2.2$, 2.0, 1.8, and 1.7, respectively. The shaded areas are sketches of the localized band.
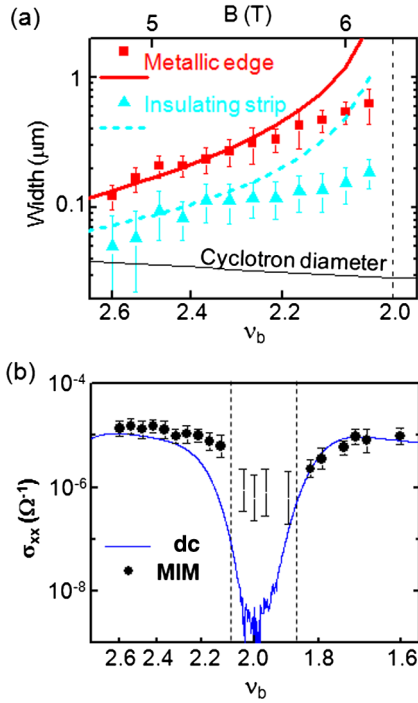
FIG. 4 (color online). (a) Widths of the measured conducting edges (squares) and insulating strips (triangles). The solid and dashed lines are results from the electrostatic calculation [3]. The semiclassical cyclotron diameter with much smaller values and incorrect trend is also plotted for comparison. (b) Comparison between the macroscopic dc transport (solid line) and microscopic microwave (solid circles) conductivity. The $\sigma_{xx}(1\ \mathrm{GHz})$ data between the two dashed lines show large uncertainties due to strong nonuniformity observed in the bulk of the 2DEG.

QHE [Figs. 3(f)–3(i)], the conducting edge states are as wide as 1 μm and the bulk electrons become highly inhomogeneous and inefficient to screen the microwave E fields. We note that the bulk is not completely insulating, presumably due to the thermal excitation at 2.3 K and the density fluctuation of the 2DEG sample. For increasing B [Figs. 3(j) and 3(k)], electrons with local densities close to $n_{\nu=2}$ are still localized by disorder in the sample. Consequently, the center of the dot appears bright in the MIM-Re channel and dim in MIM-Im. As B further increases [Fig. 3(l)], the 2DEG delocalizes and regains the ability to screen E fields, consistent with the homogeneous and metallic bulk revealed by the MIM. Such an evolution around $\nu_b = 2$ can be understood by schematics of the density profile across the dots depicted in Fig. 3(m), with a band of localized states continuously moving up in density as increasing B fields.

In Fig. 4(a), we plot the widths of the metallic and insulating strips as a function of ν_b, showing good agreements between the data and the electrostatic calculation [3] for $\nu_b > 2.2$. The deviation close to $\nu_b = 2$ may come from the density fluctuation that limits the edge channel widths. Such a quantitative comparison between theory and experiment has not been reported by other scanning techniques [8–16,24,25]. It is also clear that the width of the metallic edges cannot be estimated by the cyclotron diameter using the semiclassical skipping-orbit picture. Finally, we compare the transport $\sigma_{xx}(\mathrm{dc}) = \rho_{xx}/(\rho_{xx}^2 + \rho_{xy}^2)$ and the bulk σ_{xx} at 1 GHz in Fig. 4(b). Toward $\nu_b = 2$, the bulk conductivity drops due to the reduction of carriers in the $N = 1$ LL. The decrease of $\sigma_{xx}(1\ \mathrm{GHz})$, however, is more gradual than that of $\sigma_{xx}(\mathrm{dc})$ measured by the voltage leads, which are in equilibrium with the edges. In fact, the plummet of transport resistance is mostly from the widening of the insulatorlike strip, which drastically reduces the tunneling between the edge states and the bulk. For $|\nu_b - 2| < 0.1$, the local $\sigma_{xx}(1\ \mathrm{GHz})$ extracted from the MIM images shows very large error bars, consistent with the significant inhomogeneity observed in the bulk. In macroscopic samples, small metallic puddles are decoupled from the edges and cannot induce backscattering. The transport is thus confined to the dissipationless edge channels, resulting in a vanishing ρ_{xx} and a quantized ρ_{xy} plateau [3,4]. As the B increases sufficiently above $\nu_b = 2$, the dc conductivity matches well with the bulk σ_{xx} measured by MIM since the transport is now through the gradually delocalized 2DEG. We see that microscopically, entering and leaving an integer N are different processes. And the exact integer filling factor does not necessarily occur in the middle of the quantized plateau.

In summary, we have directly imaged the quantum Hall edge channels using a microwave impedance microscope. The widths and local conductivity of both compressible and incompressible strips can be quantitatively compared with the electrostatic model. Our results pave the way to spatially resolve other exotic physics in 2DEG, such as the fractional QHE [1], the stripe and bubble phases [26], the 2D metal-insulator transition [27], and many more.

*kejilai@stanford.edu

[1] R. E. Prange and S. M. Girvin, *The Quantum Hall Effect* (Springer, New York, 1990); S. Das Sarma and A. Pinczuk, *Perspectives in Quantum Hall Effects* (Wiley, New York, 1996).

[2] B. I. Halperin, Phys. Rev. B **25**, 2185 (1982).

[3] D. B. Chklovskii, B. I. Shklovskii, and L. I. Glazman, Phys. Rev. B **46**, 4026 (1992).

[4] C. de C. Chamon and X. G. Wen, Phys. Rev. B **49**, 8227 (1994).

[5] M. Büttiker, Phys. Rev. B **38**, 9375 (1988).

[6] T. Nakajima, Y. Kobayashi, S. Komiyama, M. Tsuboi, and T. Machida, Phys. Rev. B **81**, 085322 (2010).

[7] D. T. McClure, Y. Zhang, B. Rosenow, E. M. Levenson-Falk, C. M. Marcus, L. N. Pfeiffer, and K. W. West, Phys. Rev. Lett. **103**, 206806 (2009).

[8] K. L. McCormick, M. T. Woodside, M. Huang, M. Wu, P. L. McEuen, C. Duruoz, and J. S. Harris, Jr., Phys. Rev. B **59**, 4654 (1999).

[9] M. T. Woodside, C. Vale, P. L. McEuen, C. Kadow, K. D. Maranowski, and A. C. Gossard, Phys. Rev. B **64**, 041310 (R) (2001).

[10] N. Aoki, C. R. da Cunha, R. Akis, D. K. Ferry, and Y. Ochiai, Phys. Rev. B **72**, 155327 (2005).

[11] Y. Y. Wei, J. Weis, K. v. Klitzing, and K. Eberl, Phys. Rev. Lett. **81**, 1674 (1998).

[12] A. Yacoby, H. F. Hess, T. A. Fulton, L. N. Pfeiffer, and K. W. West, Solid State Commun. **111**, 1 (1999).

[13] S. Ilani, J. Martin, E. Teitelbaum, J. H. Smet, D. Mahalu, V. Umansky, and A. Yacoby, Nature (London) **427**, 328 (2004).

[14] G. Finkelstein, P. I. Glicofridis, S. H. Tessmer, R. C. Ashoori, and M. R. Melloch, Phys. Rev. B **61**, R16323 (2000).

[15] G. Finkelstein, P. I. Glicofridis, R. C. Ashoori, and M. Shayegan, Science **289**, 90 (2000).

[16] P. I. Glicofridis, G. Finkelstein, R. C. Ashoori, and M. Shayegan, Phys. Rev. B **65**, 121312(R) (2002).

[17] See, for example, B. T. Rosner and D. W. van der Weide, Rev. Sci. Instrum. **73**, 2505 (2002), and references therein.

[18] K. Lai, W. Kundhikanjana, M. Nakamura, M. Kawasaki, Y. Tokura, M. A. Kelly, and Z. X. Shen, Science **329**, 190 (2010).

[19] W. Kundhikanjana, K. Lai, M. A. Kelly, and Z. X. Shen, Rev. Sci. Instrum. **82**, 033705 (2011).

[20] K. Lai, W. Kundhikanjana, M. A. Kelly, and Z. X. Shen, Appl. Phys. Lett. **93**, 123105 (2008).

[21] See Supplemental Material at http://link.aps.org/supplemental/10.1103/PhysRevLett.107.176809 for details of the modeling and data analysis.

[22] We note that there is another narrow strip going through the insulator-metal transition across regions II and III in Fig. 2(a). The sharp rise of density here, however, indicates a very small strip width in the sub-10 nm scale, which results in too small a signal (below the noise floor) to be detected.

[23] The microwave imaging was performed in the contact mode to maximize the signal strength. We have observed that, after 3–4 repeated scans on the same area, the dot underneath the tip gradually changed its density, probably due to electrostatic perturbation. In this study, we only imaged each dot once and always move to fresh ones when changing conditions.

[24] A. A. Shashkin, A. J. Kent, P. A. Harrison, L. Eaves, and M. Henini, Phys. Rev. B **49**, 5379 (1994).

[25] R. J. F. van Haren, F. A. P. Blom, and J. H. Wolter, Phys. Rev. Lett. **74**, 1198 (1995).

[26] J. P. Eisenstein, M. P. Lilly, K. B. Cooper, L. N. Pfeiffer, and K. W. West, Physica (Amsterdam) **6E**, 29 (2000).

[27] E. Abrahams, S. V. Kravchenko, and M. P. Sarachik, Rev. Mod. Phys. **73**, 251 (2001).